Biexciton-Like Auger Blinking in Strongly Confined $CsPbBr_3$ Perovskite Quantum Dots

*Chenjia Mi[1], Matthew L. Atteberry[1], Varun Mapara[2], Lamia Hidayatova[1], Gavin C. Gee[1], Madalina Furis[2], Wai Tak Yip[1], Binbin Weng[3], Yitong Dong[1]**

[1]Department of Chemistry and Biochemistry, The University of Oklahoma, Norman, OK 73019, USA

[2]Homer L. Dodge Department of Physics and Astronomy, The University of Oklahoma, Norman, OK 73019, USA

[3]School of Electrical & Computer Engineering, The University of Oklahoma, Norman, OK 73019, USA

Keywords: Perovskite Quantum Dot, Blinking Suppression, Auger Recombination, Trapped Exciton, Single-Photon Emission

ABSTRACT. Single perovskite quantum dots (QDs) are notorious for their poor stability. As a result, surface defects will be generated and this will lead to trion formation that reduces fluorescence intensity, setting barriers to exploring the intrinsic exciton dynamics and the applications of perovskite QDs in single-photon sources. Here we demonstrate that strongly confined $CsPbBr_3$ perovskite QDs (SCPQDs) embedded in a matrix formed by phenethylammonium bromide exhibit suppressed trion formation and remain photostable under intense photoexcitation. The increased surface passivation and stability enables the study of multi-exciton interactions in SCPQDs. We found that, in well-passivated SCPQDs, increasing excitation rates leads to weak fluorescence intensity fluctuations accompanied by an unusual spectral blueshift in the photoluminescence. We attribute this to a biexciton-like Auger interaction between excitons and trapped excitons formed by surface lattice elastic distortions. This hypothesis is corroborated by the unique repulsive biexciton interaction in SCPQDs. Our study provides insights into the fundamental multi-exciton interactions in SCPQDs and will advance the development of quantum light sources based on perovskite QDs.

Perovskite quantum dots (QDs) have emerged as promising single-photon emitter (SPE) materials owning to their high photoluminescence (PL) quantum yields (QY) and fast radiative emission rates.[1-6] For SPEs based on single QDs, high photoexcitation rates increase the brightness at a cost of single-photon purity due to multi-exciton generations.[3, 7, 8] Strongly confined perovskite QDs (SCPQDs), whose physical sizes are smaller than the Bohr diameter of the exciton, can effectively annihilate multi-exciton emissions through Auger processes[8-11]. However, SCPQDs are notorious for their poor temporal PL stability, especially under intense photoexcitation.[8] This has significantly curtailed the understanding of intrinsic exciton dynamics and many-body interactions in perovskite QDs for its applications on SPEs.

Surfaces of perovskite QDs are susceptible to ligand losses and degradation,[12, 13] particularly when QDs are diluted and isolated from their colloidal phase for single-particle studies.[14] The resulting surface defects can promote trion formation in perovskite QDs, which subsequently reduces the PL stability via fast trion Auger recombination.[15, 16] This is more pronounced in SCPQDs due to enhanced Auger interaction and increased surface-to-volume ratio. Many efforts have been made to increase the binding affinity of surface ligands to suppress surface degradation. Zwitterionic ligands have enabled single perovskite QD studies at cryogenic temperatures.[17] Bulky lecithin ligands have been used to stabilize perovskite QDs from degradation and aggregation when being diluted.[18] Nevertheless, most single-particle studies on perovskite QDs are still limited to large, weakly-confined nanocrystals (NCs).[19, 20] In perovskite NCs, the stochastic PL intensity fluctuations (often referred to as blinking) between the exciton (ON) state and the trion (OFF) state are still prominent.[21-23] To date, the effect of multi-exciton dynamics on single-photon emissions of SCPQDs remains elusive.

Here, we report an unconventional method to prepare single SCPQDs by embedding them in a bromide salt matrix. The resulting single SCPQDs show significantly increased PLQY and photostability. This approach enables us to investigate the intrinsic blinking dynamics of single SCPQDs. We found that the single SCPQDs are essentially blinking-free under moderate photoexcitation and remain stable even when the excitation rate increases (average number of excitations, $\langle N \rangle$, up to 1.0). However, at high excitation rates, we observed PL intensity fluctuations well above the OFF state threshold, accompanied by a PL spectral blueshift. By analyzing decay dynamics of the single SCPQDs, we found that the PL lifetime only slightly decreases, along with an emerging delayed emission. These observations cannot be explained by the random exciton-trion switching found in large perovskite NCs.[3] Hence, we propose that these fluctuations in the SCPQDs arise from a biexciton-like Auger recombination between a normal exciton and a trapped exciton (TE), which is slower than trion Auger recombination. We present a microscopic model based on the conventional trion flickering theory to explain our observations and provide further supports on observed spectral blueshifts by demonstrating the unusual repulsive biexciton interactions in SCPQDs. These findings provide insights for the understanding of intrinsic exciton dynamics in SCPQDs and the development of room temperature SPEs.

Results and Discussion

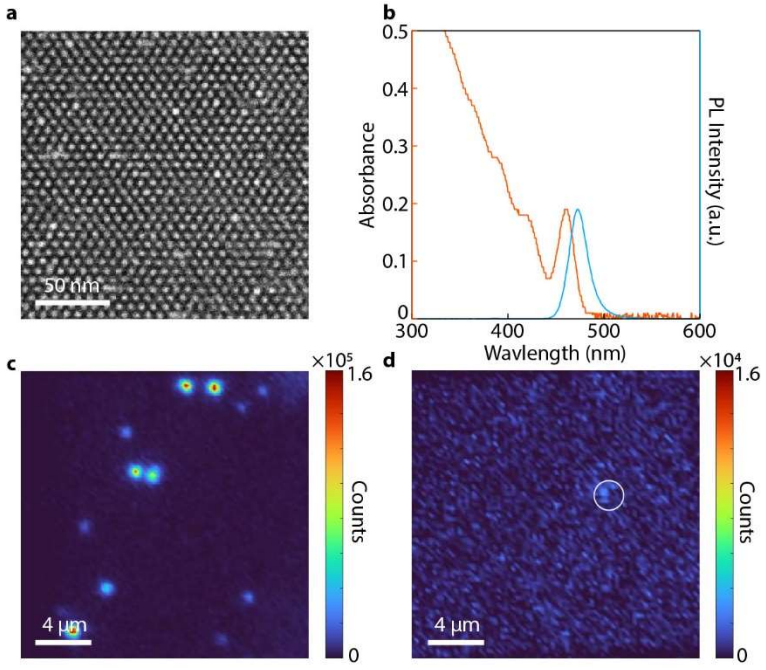

Figure 1. (a) STEM image and (b) absorption (orange) and PL (blue) spectra of colloidal $CsPbBr_3$ SCPQDs with a size of 4 nm. (c-d) Fluorescence images of the isolated single SCPQDs (c) embedded in PEABr matrix, and (d) without PEABr matrix.

$CsPbBr_3$ SCPQDs with various sizes were synthesized using previously reported method with modifications[24, 25]. The scanning transmission electron microscope (STEM) image of a 4 nm SCPQD sample (Figure 1a) reveals high size and shape uniformity, minimizing selection bias in single QD measurements. The mono-dispersity of the SCPQDs is also supported by large-scale self-assemblies observed in a STEM image (Supporting Information, Figure S1). Figure 1b shows the absorption and PL spectra of the SCPQD colloid. Due to the strong quantum confinement, the PL peak of the SCPQD shifts to 471 nm compared to the 513 nm PL peak of $CsPbBr_3$ NCs (Supporting Information, Figure S2).

To prevent surface degradation during the single-particle sample preparation, the SCPQDs were embedded in an organic ammonium bromide salt matrix. Phenethylammonium bromide (PEABr) is selected for the most optimized single-particle photostability. Briefly, a diluted SCPQD solution

in octane was spin-cast onto a layer of wet PEABr solution in dimethylformamide on a glass coverslip in a nitrogen glovebox. This method results in the SCPQDs being embedded in the PEABr matrix (Supporting Information, Figure S3 – S5). The PL characteristics of the single-particle samples were measured on a custom-built confocal fluorescence microscope. Figure 1c shows a wide-field fluorescence image of single SCPQDs in PEABr matrix. Compared to the SCPQDs without a matrix (Figure 1d), whose PL intensity is too low for reliable measurements, the PEABr matrix enhanced the PLQY of the SCPQDs by ~ 100-fold.

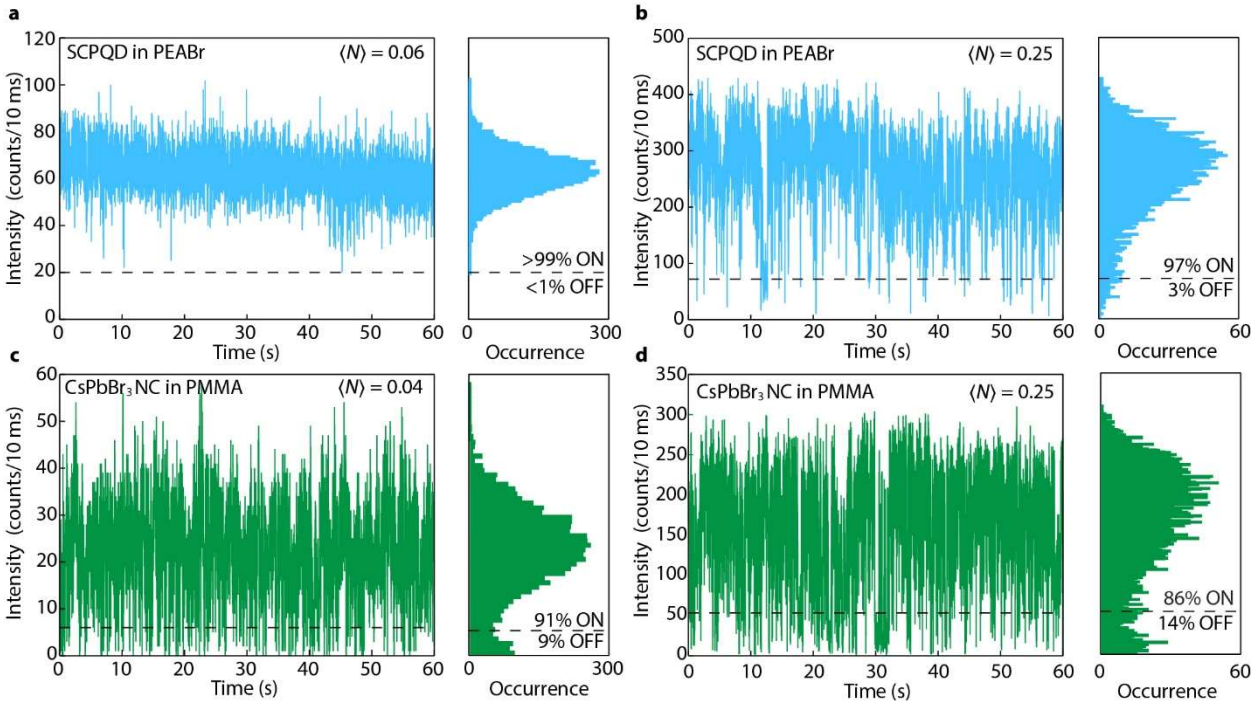

Figure 2. Time-dependent PL intensity (blinking) traces (left) and occurrence histograms (right) of (a-b) a single $CsPbBr_3$ SCPQD (PL peak centered at 471 nm, Figure 1) embedded in PEABr matrix and (c-d) a large $CsPbBr_3$ perovskite NC (PL peak centered at 513 nm, Figure S2) dispersed in PMMA at (a)(c) moderate excitation rates and at (b)(d) increased excitation rates (excitation laser: 405 nm, 4 MHz). The OFF state threshold is marked with dotted lines, determined by the exciton and the trion lifetimes.

Both SCPQDs and $CsPbBr_3$ NCs in PEABr matrix are essentially blinking-free (ON period > 99%) at moderate excitation rates, as shown in Figure 2a (and Supporting Information, Figure S6). In contrast, when dispersed in poly(methyl methacrylate) (PMMA), $CsPbBr_3$ NCs exhibit

extensive fluorescence intermittency, even at a lower excitation rate ($\langle N \rangle = 0.04$, Figure 2c). Figure 2b shows the fluorescence intensity (blinking) trace of a SCPQD at an increased excitation rate ($\langle N \rangle = 0.25$). The SCPQD exhibits low occurrence of a long-lasting OFF state and stays ON for 97% of the time (Figure 2b). In comparison, the large $CsPbBr_3$ NC has a clear distribution of the OFF state at similar excitation rates. It is worth mentioning that some SCPQDs still show finite OFF state probabilities, presumably due to the imperfect surface passivation (Supporting Information, Figure S7). The second-order correlation ($g^{(2)}$) plots show single-photon purity of 95% for the SCPQD and 85% for the large $CsPbBr_3$ NC (Supporting Information, Figure S8). The statistics of the durations of the ON and OFF states of the SCPQD are fitted to a power-law $P(t) \propto t^{-k}$ (Supporting Information, Figure S9), which yield $k_{ON} = 0.8$, and $k_{OFF} = 1.9$. The fast decay of the OFF time probability distribution indicates that the SCPQD remain emissive for most of the time.

Although the OFF state is suppressed in the SCPQDs protected by the PEABr matrix, a fluorescence intensity fluctuation well above the OFF state was observed at an increased excitation rate ($\langle N \rangle = 0.25$). This can be better visualized in the occurrence histogram in Figure 2b. Such a fluctuation has been observed in several SCPQDs with various sizes (Supporting Information, Figure S10) at $\langle N \rangle = 0.10$, but disappears after reducing the excitation rate to $\langle N \rangle = 0.02$ (Supporting Information, Figure S11). In contrast, the large $CsPbBr_3$ NC in PMMA exhibits fluctuations between the ON and OFF states even at low excitations rates. The PL intensity fluctuation in large $CsPbBr_3$ NCs has been interpreted as a random switching between exciton and trion emissions. To verify the validity of the trion model and to distinguish the intensity fluctuation in SCPQDs from the trion-induced blinking, we used a smaller bin size (1 ms) to plot the blinking traces (Supporting Information, Figure S12).[26] While the large $CsPbBr_3$ exhibits binary blinking

behavior with manifest OFF states, similar to what is commonly seen in CdSe QDs (Supporting Information, Figure S13), the intensity fluctuation behavior of the SCPQD persists. These findings suggest that the PL intensity fluctuations in the SCPQD cannot be explained by the typical trion model.[27]

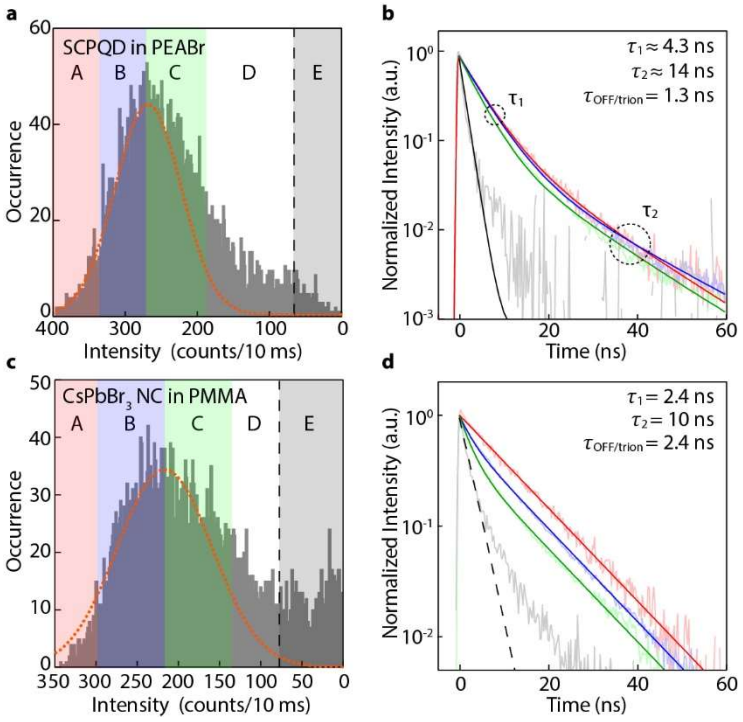

Figure 3. Occurrence histograms of the PL intensity of (a) the SCPQD in PEABr and (c) the large $CsPbBr_3$ NC in PMMA, at $\langle N \rangle$ = 0.25. The color-coded intensity ranges are used to extract intensity-dependent PL decay curves in (b) and (d), respectively. For clarity, the decay curves extracted range A – C with bi-exponential fits are shown, along with representative OFF state decay curves only fitted for the trion component (black). The decay curves extracted from range D – E and fits are given in Figure S15.

To explore the new blinking behavior of the SCPQDs, we generated fluorescence lifetime-intensity distribution (FLID) heatmaps by extracting the PL lifetime at each intensity level from mono-exponential fits (Supporting Information, Figure S14). A non-linear correlation is observed between the PL intensities and lifetimes, implying that an Auger mechanism is involved.[27] However, mono-exponential fits used in the FLID heatmaps cannot fully reveal the complex decay dynamics. To further analyze the dynamics of the unusual emission intensity fluctuation in

SCPQDs, we extracted the PL decay dynamics at various PL intensity ranges, as color-coded in the intensity histograms in Figure 3a and 3c. The extracted PL decay traces from all ON levels are shown in Figure 3b and 3d and are fitted with bi-exponential decay functions. All time constants (τ) and pre-exponential factors (K) obtained from the fittings are summarized in Table 1. The decay curves of the OFF states are extracted (range E in Figure 3a for the SCPQD, and the selected range in Figure S15 for the $CsPbBr_3$ NC), and only the fast component was shown to reflect the lifetime of trions. The slow components with a time constant close to that of the normal excitons are attributed to small fractions of exciton emissions inside the bins. The decay curves extracted from range D and E are shown in Supporting Information, Figure S16.

Table 1. Time constants and fractions obtained from bi-exponential fittings in Figure 3.

Range	SCPQD in PEABr		$CsPbBr_3$ NC in PMMA[1]	
	τ_1 (K_1)	τ_2 (K_2)	τ_1 (K_1)	τ_2 (K_2)
A	4.7 ns (86%)	13 ns (14%)	-	10 ns (100%)
B	4.8 ns (91%)	15 ns (9%)	2.4 ns (35%)	10 ns (65%)
C	4.0 ns (89%)	13 ns (11%)	2.4 ns (57%)	10 ns (43%)
D	1.5 ns (83%)	6.0 ns (17%)	2.4 ns (74%)	10 ns (26%)
E	1.3 ns (100%)	-	2.4 ns (34%)[2]	10 ns (6%)

[1] Global fitting is performed with shared time constants for the PL decays of the $CsPbBr_3$ NC in PMMA.

[2] The PL decay curve possess an additional fast component of 0.5 ns (60%), which is attributed to the instrument response function.

The PL decay curves extracted from range A to C of the SCPQD (Figures 3a and 3b) exhibit nearly identical decay dynamics, with similar time constants and fractions for both the fast (~ 4.3 ns) and slow (~ 14 ns) components (Table 1). It is noticeable that the lifetime of the trion is 1.3 ns (range E) and is much faster than the lifetime of the short decay components (4.0 – 4.7 ns) obtained for range A-C. This indicates that there is little to no trion emission contributions in the majority of the ON levels. In comparison, the PL decay curves of the $CsPbBr_3$ NC from range A to D in

Figure 3a contain two components with the same time constants but increasing contributions from the fast component. The time constants of the fast (2.4 ns) and slow (10 ns) components agree well with the decay lifetimes of trions and excitons, respectively.[22, 23, 28-32] These behaviors are consistent with trion blinking model.[31]

The different PL dynamics clearly indicate that intensity fluctuations in SCPQD are not induced by trions. Interestingly, in Figure 3d and Table 1, the time constant of the fast decay component (~ 4.3 ns) is slightly shorter than the radiative lifetime of excitons (6.4 ns, Figure 4c) but 3 times longer than the lifetime of trions (1.3 ns), while the slow component possesses a longer lifetime than that of the excitons. This is inconsistent with the conventional trion model, where a charged QD can generate trions that undergo fast Auger non-radiative recombination. To fully explain our observations, a non-charging model include multi-excitonic states need to be introduced. Trapped excitons (TEs) – the electron-hole pair are localized and stabilized by the lattice polarons – have been proposed in $CsPbBr_3$ perovskites.[33-38] In our SCPQDs, given the softness of the surface lattices and the strong exciton-surface interaction promoted by the size confinement, we propose that exciton-surface lattice polarons can form, which lead to the TE formation.

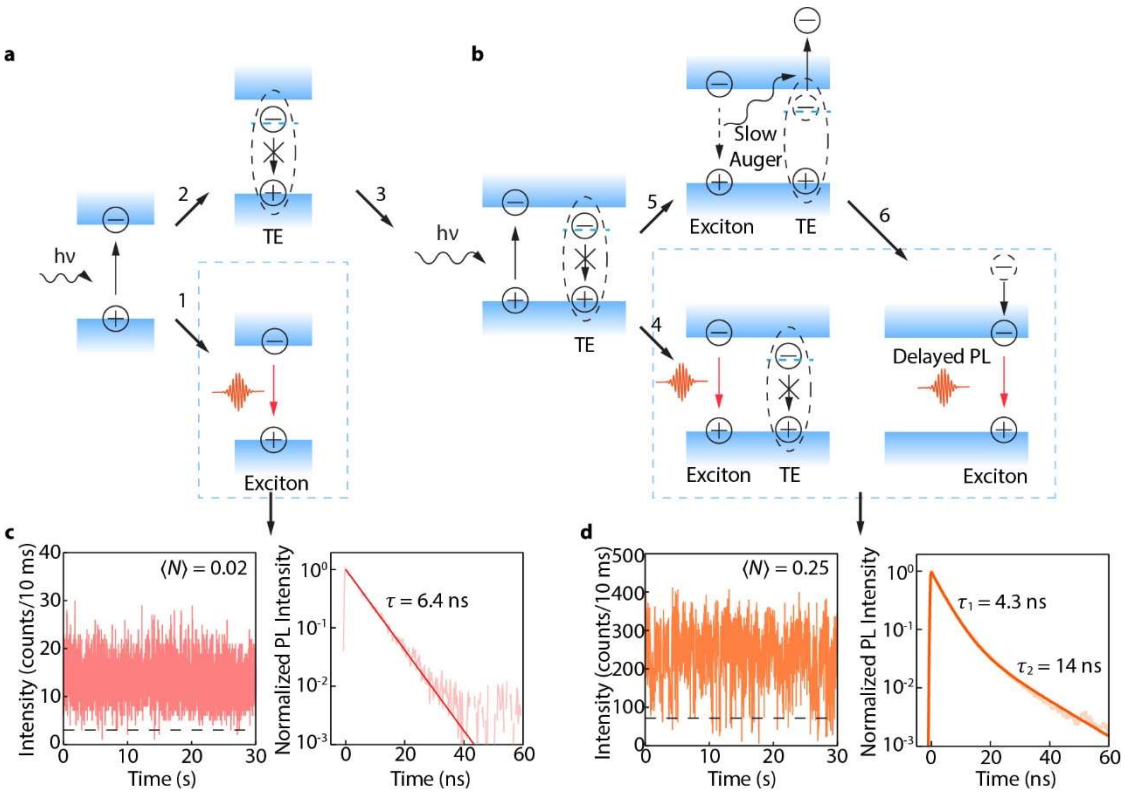

Figure 4. (a) Scheme of proposed biexciton-like Auger interaction between exciton and trapped exciton (TE). When an exciton is generated in a QD, it will emit a photon (route 1) or be trapped (route 2). (b) The QD that contains a TE can be excited again (route 3), resulting in an exciton-TE pair. The exciton can emit a photon under the influence of the TE (route 4). Alternatively, biexciton-like Auger recombination can happen in the exciton-TE pair (route 5). Then the TE will be de-trapped, resulting in a recovered normal exciton (route 6) accompanied by delayed PL. (c) Blinking and PL decay trace at low excitation rate ($\langle N \rangle$ = 0.02), representing (a). (d) Blinking and PL decay trace at high excitation rate ($\langle N \rangle$ = 0.25), where intensity fluctuation and delayed PL can be observed, representing (b).

Here we present a microscopic model to explain the blinking behavior discovered in the SCPQD (Figure 4). In the model, an exciton has a finite probability of forming a TE (route 2) before emitting a photon (route 1), as shown in Figure 4a. The TE possesses a lower energy compared to a normal exciton and a long lifetime, and thus is generally non-emissive. This is supported by the observation of a weak, broad emission feature with a decay time of ~ 1 μs from SCPQDs in low-temperature PL measurements (Supporting Information, Figure S17). At high excitation rates, another exciton can be created in the QD with a TE in it (route 3), generating an exciton-TE pair

(Figure 4b). The exciton-TE pair is biexciton-like and can undergo Auger recombination (route 5). However, due to the screening effect introduced by the surface lattice distortion, the Auger process is slow. As a result, the exciton can still recombine radiatively under the influence of the TE (route 4). Since the Auger recombination is slow, the exciton emission is only slightly quenched. This is in good agreement of the ~ 4.3 ns decay time found in Figure 3d. Additionally, an exciton can be recovered via the exciton-TE Auger interaction (route 6) and then recombine radiatively, leading to the delayed PL observed in Figures 3b and 4d.

Unlike the trion-induced intensity fluctuation, the PL intensity fluctuation induced by exciton-TE pairs only happen at high excitation rates. As shown in Figures 4c and 4d, at a low excitation rate ($\langle N \rangle = 0.02$), a mono-exponential PL decay is observed (Figure 4c); when the excitation rate increases ($\langle N \rangle = 0.25$), the PL intensity starts to fluctuate above the OFF state threshold, and the PL decay becomes bi-exponential (Figure 4d). This excitation rate dependence in the PL of single SCPQDs has been reproducibly observed (Supporting Information, Figure S18). The excitation rate dependent blinking behavior and decay dynamics are consistent with the emission mechanisms depicted in Figures 4a and 4b. It is worth to note that since TE is not emissive and the emissions in all three routes shown in Figure 4 come from single excitons, the single-photon purity remains high in the SCPQD (~ 95%, Figure S8).

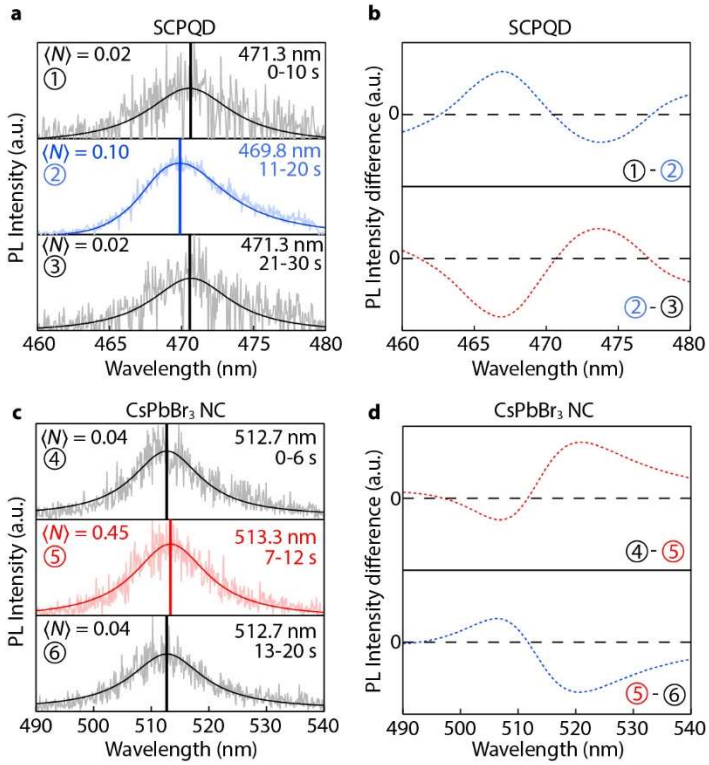

Figure 5. (a) Excitation rate dependent single-particle PL spectra of a SCPQD, measured continuously at excitation rates switching between ⟨*N*⟩ = 0.02 and 0.10. (b) The difference of the PL spectra in (a). (c) Excitation rate dependent single-particle PL spectra of a $CsPbBr_3$ NC in PMMA, measured continuously at excitation rates switching between ⟨*N*⟩ = 0.04 and 0.45. (d) The difference of the PL spectra in (c). The spectra at low excitation rates in 1, 3, 4 and 6 are fitted with Lorentzian function (solid curves). The shifted spectra at high excitation rates deviates from Lorentzian due to mixed emission states, and the solid curves in 2 and 5 are smoothed spectra for visual guides. The vertical strokes mark the peak positions.

To gain more insights into the proposed biexciton-like Auger interaction between the exciton and TE, we measured excitation rate dependent single-particle PL spectra. Figure 5a shows the excitation rate dependent emission spectra of a SCPQD. Surprisingly, we observed a reversible blueshift in the PL spectra with increased excitation rate (⟨*N*⟩ = 0.10). This spectral shift is better visualized in the differential PL spectra shown in Figure 5b. In stark contrast, the PL spectra from a large $CsPbBr_3$ NC shows a slight and reversible redshift at an increased excitation rate (Figure 5c-d). This spectral redshift is tentatively attributed to the increased contribution from the attractive interaction in trions in large $CsPbBr_3$ NCs.[16, 39]

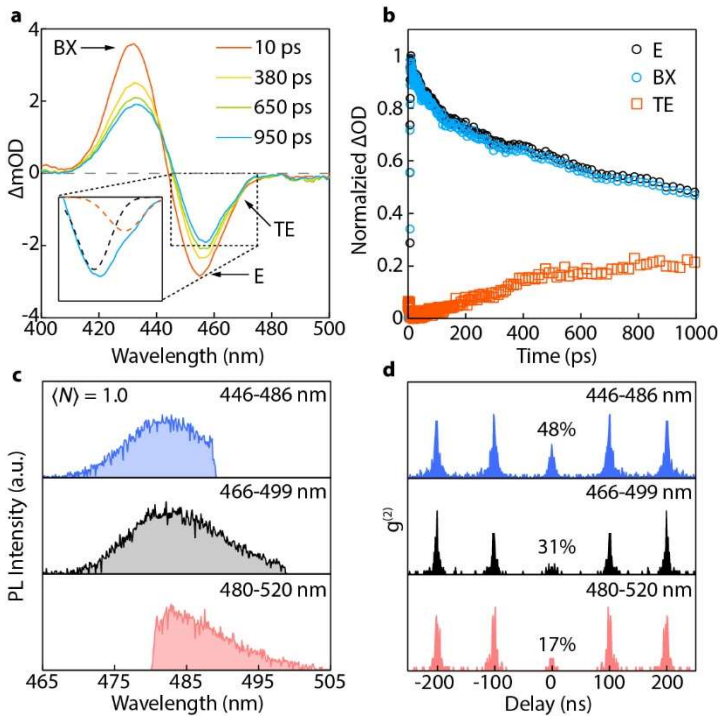

Figure 6. (a) Transient absorption spectra measured at various delay times. Exciton (E) bleach, induced absorption (BX) and trapped exciton (TE) bleach features are observed. (b) The decay dynamics of E (black), BX (blue) and TE (orange) extracted from the transient absorption spectra. (c) Spectrally selected single SCPQD PL spectra measured at the excitation rate of ⟨*N*⟩ = 1.0. (d) Spectral resolved second-order correlation statistics.

To verify our proposed model, it is necessary to assess the polarity of the biexciton interaction in SCPQDs. While biexciton interactions in perovskite QDs have been intensively investigated,[19, 40-43] most of the studies are limited to large perovskite NCs with weak quantum confinement due to the challenges in the synthesis and passivation of the SCPQDs. Although attractive biexciton interactions are frequently reported in perovskite NCs,[28, 44, 45] repulsive biexciton interactions have also been discovered in perovskite QDs of different sizes.[46, 47] To confirm the polarity of the biexciton interaction in our SCPQDs, we performed transient absorption measurements on a thin-film sample. As shown in Figure 6a, an induced absorption peak appears at higher energy, which shares the same dynamic as the exciton bleach recovery (Figure 6b). This observation aligns with previously discovered TA features in similar SCPQDs[48] and is attributed to repulsive biexciton

interactions.[47] Additionally, a new bleach peak emerges at the lower energy side of the band-edge exciton bleach peak, which we attribute to the formation of TEs. The slow dynamics of TEs agree well with the model proposed in Figure 4.

To further support the repulsive biexciton interaction in our SCPQDs, we also performed spectral resolved second-order correlation measurements. As shown in Figure 6c, emissions of a SCPQD were spectrally selected using optical filters to build spectral resolved antibunching statistics. A high excitation rate ($\langle N \rangle$ = 1.0) was used on a slightly larger (~ 4.5 nm) SCPQD to intentionally generate biexcitons. The $g^{(2)}(0)$ value extracted from the full spectral range is ~ 31%. When higher energy emissions were selected, the corresponding $g^{(2)}(0)$ values increased to ~ 48% (Figure 6d blue), showing that the biexciton emissions mainly reside on the high energy side of the spectrum. Indeed, when lower energy emissions were selected, the corresponding $g^{(2)}(0)$ value decreased to ~ 17% (Figure 6d red). The spectral resolved single-particle $g^{(2)}$ analyses are corroborated with power-dependent PL measurements of perovskite QD thin-films, which revealed similar size-dependent spectral shifts (Supporting Information, Figure S19). The unusual repulsive biexciton interaction discovered in our SCPQDs is consistent with the blueshift in the single-particle spectra caused by the biexciton-like exciton-TE interaction.

Conclusion

In conclusion, our study has revealed that trion formation is significantly suppressed in SCPQDs that are well-passivated in a PEABr matrix. Through the PL emission dynamic analyses, we have shown that TE can form in SCPQDs and undergo slow Auger interaction with normal excitons. This interaction leads to PL intensity fluctuations and spectral blueshifts in SCPQDs at increased excitation rates. The proposed exciton-TE Auger interaction in SCPQDs is further supported by the unusual repulsive biexciton interaction. These findings suggest that SCPQDs are promising to

serve as non-blinking SPE materials. Furthermore, the understanding of new exciton dynamics in SCPQDs can advance our knowledge of the emerging optical properties of perovskite QDs and accelerate their adoption in quantum photonic applications.

Methods

Materials

Core-shell CdSe/ZnS QDs with PL peak centered at 470 nm (> 80% PLQY) and 650 nm (~ 100% QY) were purchased from NNCrystal. NaBr, $PbBr_2$ and $ZnBr_2$ were purchased from Sigma-Aldrich; Cs_2CO_3 was purchased from Alfa-Aesar; Poly(methyl methacrylate) (PMMA, MW ~ 550,000) was purchased from Beantown Chemical; Phenethylammonium bromide (PEABr), isopropylammonium bromide (IPABr) and n-butylammonium bromide were purchased from Greatcell Solar Materials. Oleylamine (OAm) and oleic acid (OA) were purchased from Sigma-Aldrich; 1-Octadecene (ODE) was purchased from Thermo Fisher. Hexanes, anhydrous octane, anhydrous toluene and anhydrous *N,N*-dimethylformamide (DMF) were purchase from Sigma-Aldrich; Acetone and isopropanol were purchased from Fisher. All chemical materials were used as received.

Colloidal $CsPbBr_3$ SCPQD Synthesis

The $CsPbBr_3$ SCPQDs were synthesized using a reported method with modifications[24]. Briefly, 300 mg of Cs_2CO_3 in a 25 mL 3-necked flask, 600 mg of $PbBr_2$, and 1400 mg of $ZnBr_2$ in a 250 mL 3-necked flask were weighed in a glove box protected by nitrogen. To prepare the Cs oleate precursor, 1.2 mL of OA, 3.2 mL of ODE were mixed with the Cs_2CO_3 followed by vacuum drying at room temperature for over 30 min. The mixture was heated to 140 °C for 10 min and the temperature was kept at 120 °C before use. In the flask containing $PbBr_2$ and $ZnBr_2$, 14 mL OA, 14 mL OAm, and 25 mL ODE were added. The mixture was dried under vacuum at 150 °C for 17 min. Then the mixture was kept at different reaction temperatures ranging from 80 – 120 °C under a nitrogen atmosphere for different sized SCPQDs. The reaction was triggered by injecting 2.5 mL of Cs precursor into the mixture, maintained at the same temperature for 3 min and then quenched

using an ice-water bath. Non-reacted solids were removed by centrifuging the mixture at 7800 rpm for 10 min.

The reacted mixture that contains SCPQD colloids were centrifuged again after standing still for at least 24 hours to remove unreacted precursors. To wash the SCPQD particles, ~ 50 mL of acetone was added to the mixture followed by vigorously shaking. Upon formation of turbidity, the mixture was centrifuged again to collect the particles as precipitants. The SCPQDs were re-dispersed in octane for storage and further use.

Coverslip Cleaning

Coverslips were loaded on a PTFE rack and sonicated in the following solvents each for 40 min at room temperature: 1. DI water with 0.1% (v/v) Triton-X 100; 2. DI water; 3. Acetone; 4. Isopropanol. The coverslips were rinsed 6 times with DI water between step 1 and 2. After sonication, the coverslips were dried in an oven for 10 min and then stored in a dust-free container. Before sample preparation, the coverslips were conditioned using a UV-ozone cleaner for 30 min, then sent into the glovebox.

Single-Particle Sample Preparation

CdSe/ZnS QD stock suspension was diluted by 4 orders of magnitude using anhydrous toluene containing 0.4% (m/m) PMMA. 10 μL of the diluted II-VI QD suspension was spin-coated (5000 rpm, 1 min, dynamic) onto a pre-cleaned coverslip in a nitrogen glovebox. The coverslip was then annealed at 70 °C for 2 min and encapsulated using optical adhesives.

Large $CsPbBr_3$ NCs were synthesized using previously reported methods.[25] The resulting stock colloid was diluted by 5 to 6 orders of magnitude using anhydrous toluene containing 1.0% (m/m) PMMA. 150 μL of the diluted NC suspension was spin-cast at onto a pre-cleaned coverslip 5000

rpm for 1 min in a nitrogen glovebox. The coverslip was then annealed at 70 °C for 2 min and encapsulated using optical adhesives.

$CsPbBr_3$ SCPQD colloid was diluted by 4 to 5 orders of magnitude using anhydrous octane solution saturated with n-butylammonium bromide. To prepare SCPQD in PEABr matrix sample, 150 μL of PEABr DMF solution (250 mg/mL) was dropped onto a coverslip then spin-cast using a two-step procedure: first at 1000 rpm for 10 s and then at 5000 rpm for 1 min. After 20 s of spinning when the spin rate reaches 5000 rpm, 10 μL of the diluted SCPQD colloid was dropped onto the coverslip. The sample coverslip was annealed at 70 °C for 2 min and then encapsulated using optical adhesives. SCPQDs in other matrices (IPABr, NaBr-PEABr) were prepared similarly (see Supporting Information, Figure S20 for the measured blinking traces).

Single-Particle PL Measurements

The emission dynamics of a single QD was measured using a custom-designed wide-field/confocal microscope. The excitation light source was an LDH-D-C-405 laser head driven by a Sepia PDL-828 driver from Picoquant, operating at either 4 MHz pulsed mode or continuous-wave mode (unless otherwise specified). After being attenuated with neutral density filters, the laser was reshaped and guided by a single mode fiber and sent through the epi-illuminating port of Nikon Eclipse TE200 inverted microscope, reflected by a 425 nm long-pass dichroic mirror, through a Nikon CFI Super Fluor 100X objective to the sample. The sample emission was collected with the same objective and sent through the dichroic filter, a tube lens, a pair of slits in the X-Y direction at the intermediate image plane (as confocal pinhole), a collimating lens, a set of filters (a 405 nm notch filter, a 425 nm long-pass filter, and a selected bandpass filter), and then into the detection systems. A scheme of the optical system can be found in Supporting Information, Figure S21.

The fluorescence images of QDs were obtained using an Andor iXon DV897 EMCCD. Spectra of QDs were obtained using a spectrograph that contains an Andor Shamrock 500i monochromator and an Andor iXon Ultra897 EXF EMCCD. For photon counting, the emissions were split by a non-polarizing 50:50 beam splitter, collected by two Hamamatsu C11202-100 single-photon avalanche diodes (SPADs), and recorded with a Picoquant HydraHarp 400 module using time-tagged time-resolved (TTTR) mode. Two Excelitas SPCM-AQRH-15-FC SPADs were also used for earlier experiments. PL intensities were corrected with the wavelength dependent response curves of the SPADs.

Transient Absorption Measurements

UV pump/white light probe transient absorption spectra were recorded every 250 fs for a time window of 1 ns using a HELIOS transient absorption spectrometer from Ultrafast Systems. The white light probe was generated using the 532 nm frequency doubled output of a 2 kHz HYPERION Yb amplifier (also Ultrafast Systems) focused on a sapphire crystal inside the HELIOS spectrometer. The 350 nm UV pump was provided by the tunable output of an Ultrafast Systems Optical Parametric Amplifier (OPA) pumped by the same amplifier.

Low Temperature PL Measurements

The SCPQD colloid was spin-cast onto a sapphire substrate with PEABr matrix, similarly to the single-particle samples, except concentrated stock colloid was used. The as-prepared sample was then vacuum dried overnight and loaded into an ARS GMX-20-OM cryostat. The sample PL and lifetime were then measured at room temperature and at 8 K. The sample temperature was measured with a free-range probe stuck to the sapphire substrate. The excitation pulse was provided by the same OPA in the transient absorption measurements, and focused to the sample

with an achromatic lens. The PL signal is collected by the same lens for spectra and lifetime measurements.

Data Processing

Data acquired from the time correlation module running at TTTR mode were processed as follows. The data file was translated and processed using customized MATLAB codes from the Picoquant demo code. The codes can be distributed upon request. The second-order correlation ($g^{(2)}$) of the PL signals from the two SPADs was obtained with previously reported methods[49].

FLID heatmaps were generated by interrogating the photon arrival times, respecting to the excitation pulses, of all the photon events at each counts level in the blinking trace. The photon arrival times were then used to build histograms to generate PL decay curves. The decay curve of each counts level was then corrected for baseline based on the average counts appeared in the time range from -10% to -2% of the repetition time, respecting to the excitation pulse (defined as time zero). The corrected curves were fit with a mono-exponential function to extract lifetimes.

ASSOCIATED CONTENT

Supporting Information.

The Supporting Information is free of charge at https://pubs.acs.org/doi/10.1021/xxxxxxx

Additional STEM images, fluorescence microscopy images, second-order correlation plots, ensemble absorption and PL spectra, blinking traces, occurrence histograms, FLID heatmaps, duration statistics, single of various states in SCPQDs and large $CsPbBr_3$ NCs, time-dependent PL spectra of SCPQDs and II-VI QDs; Scheme of the fluorescence microscope setup.

AUTHOR INFORMATION

Corresponding Author

Yitong Dong – Department of Chemistry and Biochemistry, the University of Oklahoma, Norman, OK 73019, USA

Authors

Chenjia Mi – Department of Chemistry and Biochemistry, the University of Oklahoma, Norman, OK 73019, USA

Matthew L. Atteberry – Department of Chemistry and Biochemistry, the University of Oklahoma, Norman, OK 73019, USA

Varun Mapara – Homer L. Dodge Department of Physics and Astronomy, the University of Oklahoma, Norman, OK 73019, USA

Lamia Hidayatova – Department of Chemistry and Biochemistry, the University of Oklahoma, Norman, OK 73019, USA

Gavin C. Gee – Department of Chemistry and Biochemistry, the University of Oklahoma, Norman, OK 73019, USA

Wai Tak Yip – Department of Chemistry and Biochemistry, the University of Oklahoma, Norman, OK 73019, USA

Madalina Furis – Homer L. Dodge Department of Physics and Astronomy, the University of Oklahoma, Norman, OK 73019, USA

Binbin Weng – School of Electrical & Computer Engineering, the University of Oklahoma, Norman, OK 73019, USA

Author Contributions

C.M. and Y.D. designed the study, performed the experiments, analyzed the data and wrote the manuscript. M.L.A., L.H. and B.W. assisted with sample preparation. V.M. and M.F. assisted with transient absorption and low temperature PL experiments. G.C.G. assisted with single-particle PL measurements. All authors contributed to the manuscript and have given approval to the submission of the manuscript.

Notes

The authors declare no competing financial interest.

ACKNOWLEDGMENT

Financial support for this work was provided by the University of Oklahoma startup funds and by a grant from the Research Council of the University of Oklahoma Norman Campus. We acknowledge the support of the Vice President for Research and Partnerships of the University of Oklahoma. Use of the TAMU Materials Characterization Facility (RRID: SCR_022202) and Dr. Sisi Xiang are acknowledged. We thank Dr. Julian Sabisch and the Samuel Roberts Noble Microscopy Laboratory at the University of Oklahoma for the TEM measurements and help on image processing. We thank Dr. Gang Yang and the Microfabrication Research & Education Center (MREC) cleanroom for the assistance on single particle sample preparation. We thank Kanika Parashar for the assistance on single particle sample preparation and measurements.

REFERENCES

(1) Aharonovich, I.; Englund, D.; Toth, M. Solid-state single-photon emitters, *Nat. Photon.* **2016**, *10*, 631-641. https://doi.org/10.1038/nphoton.2016.186

(2) Utzat, H.; Sun, W.; Kaplan, A. E. K.; Krieg, F.; Ginterseder, M.; Spokoyny, B.; Klein, N. D.; Shulenberger, K. E.; Perkinson, C. F.; Kovalenko, M. V.; Bawendi, M. G. Coherent single-photon emission from colloidal lead halide perovskite quantum dots, *Science* **2019**, *363*, 1068-1072. https://www.science.org/doi/abs/10.1126/science.aau7392

(3) Park, Y.-S.; Guo, S.; Makarov, N. S.; Klimov, V. I. Room Temperature Single-Photon Emission from Individual Perovskite Quantum Dots, *ACS Nano* **2015**, *9*, 10386-10393. https://doi.org/10.1021/acsnano.5b04584

(4) Dey, A.; Ye, J.; De, A.; Debroye, E.; Ha, S. K.; Bladt, E.; Kshirsagar, A. S.; Wang, Z.; Yin, J.; Wang, Y.; Quan, L. N.; Yan, F.; Gao, M.; Li, X.; Shamsi, J.; Debnath, T.; Cao, M.; Scheel, M. A.; Kumar, S.; Steele, J. A.; Gerhard, M.; Chouhan, L.; Xu, K.; Wu, X.-g.; Li, Y.; Zhang, Y.; Dutta, A.; Han, C.; Vincon, I.; Rogach, A. L.; Nag, A.; Samanta, A.; Korgel, B. A.; Shih, C.-J.; Gamelin, D. R.; Son, D. H.; Zeng, H.; Zhong, H.; Sun, H.; Demir, H. V.; Scheblykin, I. G.; Mora-Seró, I.; Stolarczyk, J. K.; Zhang, J. Z.; Feldmann, J.; Hofkens, J.; Luther, J. M.; Pérez-Prieto, J.; Li, L.; Manna, L.; Bodnarchuk, M. I.; Kovalenko, M. V.; Roeffaers, M. B. J.; Pradhan, N.; Mohammed, O. F.; Bakr, O. M.; Yang, P.; Müller-Buschbaum, P.; Kamat, P. V.; Bao, Q.; Zhang, Q.; Krahne, R.; Galian, R. E.; Stranks, S. D.; Bals, S.; Biju, V.; Tisdale, W. A.; Yan, Y.; Hoye, R. L. Z.; Polavarapu, L. State of the Art and Prospects for Halide Perovskite Nanocrystals, *ACS Nano* **2021**, *15*, 10775-10981. https://doi.org/10.1021/acsnano.0c08903

(5) Senellart, P.; Solomon, G.; White, A. High-performance semiconductor quantum-dot single-photon sources, *Nat. Nanotechnol.* **2017**, *12*, 1026-1039. https://doi.org/10.1038/nnano.2017.218

(6) Rainò, G.; Nedelcu, G.; Protesescu, L.; Bodnarchuk, M. I.; Kovalenko, M. V.; Mahrt, R. F.; Stöferle, T. Single Cesium Lead Halide Perovskite Nanocrystals at Low Temperature: Fast Single-Photon Emission, Reduced Blinking, and Exciton Fine Structure, *ACS Nano* **2016**, *10*, 2485-2490. https://doi.org/10.1021/acsnano.5b07328

(7) Hsu, B.-W.; Chuang, Y.-T.; Cheng, C.-Y.; Chen, C.-Y.; Chen, Y.-J.; Brumberg, A.; Yang, L.; Huang, Y.-S.; Schaller, R. D.; Chen, L.-J.; Chuu, C.-S.; Lin, H.-W. Very Robust Spray-Synthesized CsPbI3 Quantum Emitters with Ultrahigh Room-Temperature Cavity-Free Brightness and Self-Healing Ability, *ACS Nano* **2021**, *15*, 11358-11368. https://doi.org/10.1021/acsnano.1c00733

(8) Boehme, S. C.; Bodnarchuk, M. I.; Burian, M.; Bertolotti, F.; Cherniukh, I.; Bernasconi, C.; Zhu, C.; Erni, R.; Amenitsch, H.; Naumenko, D.; Andrusiv, H.; Semkiv, N.; John, R. A.; Baldwin, A.; Galkowski, K.; Masciocchi, N.; Stranks, S. D.; Rainò, G.; Guagliardi, A.; Kovalenko, M. V. Strongly Confined CsPbBr3 Quantum Dots as Quantum Emitters and Building Blocks for Rhombic Superlattices, *ACS Nano* **2023**, *17*, 2089-2100. https://doi.org/10.1021/acsnano.2c07677

(9) Lounis, B.; Bechtel, H. A.; Gerion, D.; Alivisatos, P.; Moerner, W. E. Photon antibunching in single CdSe/ZnS quantum dot fluorescence, *Chem. Phys. Lett.* **2000**, *329*, 399-404. https://www.sciencedirect.com/science/article/pii/S0009261400010423

(10) Brokmann, X.; Messin, G.; Desbiolles, P.; Giacobino, E.; Dahan, M.; Hermier, J. P. Colloidal CdSe/ZnS quantum dots as single-photon sources, *New J. Phys.* **2004**, *6*, 99. https://dx.doi.org/10.1088/1367-2630/6/1/099

(11) Zhu, C.; Marczak, M.; Feld, L.; Boehme, S. C.; Bernasconi, C.; Moskalenko, A.; Cherniukh, I.; Dirin, D.; Bodnarchuk, M. I.; Kovalenko, M. V.; Rainò, G. Room-Temperature, Highly Pure Single-Photon Sources from All-Inorganic Lead Halide Perovskite Quantum Dots, *Nano Letters* **2022**, *22*, 3751-3760. https://doi.org/10.1021/acs.nanolett.2c00756

(12) Almeida, G.; Infante, I.; Manna, L. Resurfacing halide perovskite nanocrystals, *Science* **2019**, *364*, 833-834. https://www.science.org/doi/abs/10.1126/science.aax5825

(13) De Roo, J.; Ibáñez, M.; Geiregat, P.; Nedelcu, G.; Walravens, W.; Maes, J.; Martins, J. C.; Van Driessche, I.; Kovalenko, M. V.; Hens, Z. Highly Dynamic Ligand Binding and Light Absorption Coefficient of Cesium Lead Bromide Perovskite Nanocrystals, *ACS Nano* **2016**, *10*, 2071-2081. https://doi.org/10.1021/acsnano.5b06295

(14) Rainò, G.; Landuyt, A.; Krieg, F.; Bernasconi, C.; Ochsenbein, S. T.; Dirin, D. N.; Bodnarchuk, M. I.; Kovalenko, M. V. Underestimated Effect of a Polymer Matrix on the Light Emission of Single CsPbBr3 Nanocrystals, *Nano Lett.* **2019**, *19*, 3648-3653. https://doi.org/10.1021/acs.nanolett.9b00689

(15) Kanemitsu, Y. Trion dynamics in lead halide perovskite nanocrystals, *The Journal of Chemical Physics* **2019**, *151*, 170902. https://aip.scitation.org/doi/abs/10.1063/1.5125628

(16) Nakahara, S.; Tahara, H.; Yumoto, G.; Kawawaki, T.; Saruyama, M.; Sato, R.; Teranishi, T.; Kanemitsu, Y. Suppression of Trion Formation in CsPbBr3 Perovskite Nanocrystals by

Postsynthetic Surface Modification, *J. Phys. Chem. C* **2018**, *122*, 22188-22193. https://doi.org/10.1021/acs.jpcc.8b06834

(17) Krieg, F.; Ochsenbein, S. T.; Yakunin, S.; ten Brinck, S.; Aellen, P.; Süess, A.; Clerc, B.; Guggisberg, D.; Nazarenko, O.; Shynkarenko, Y.; Kumar, S.; Shih, C.-J.; Infante, I.; Kovalenko, M. V. Colloidal CsPbX3 (X = Cl, Br, I) Nanocrystals 2.0: Zwitterionic Capping Ligands for Improved Durability and Stability, *ACS Enery Lett.* **2018**, *3*, 641-646. https://doi.org/10.1021/acsenergylett.8b00035

(18) Krieg, F.; Ong, Q. K.; Burian, M.; Rainò, G.; Naumenko, D.; Amenitsch, H.; Süess, A.; Grotevent, M. J.; Krumeich, F.; Bodnarchuk, M. I.; Shorubalko, I.; Stellacci, F.; Kovalenko, M. V. Stable Ultraconcentrated and Ultradilute Colloids of CsPbX3 (X = Cl, Br) Nanocrystals Using Natural Lecithin as a Capping Ligand, *J. Am. Soc. Chem.* **2019**, *141*, 19839-19849. https://doi.org/10.1021/jacs.9b09969

(19) Tamarat, P.; Hou, L.; Trebbia, J.-B.; Swarnkar, A.; Biadala, L.; Louyer, Y.; Bodnarchuk, M. I.; Kovalenko, M. V.; Even, J.; Lounis, B. The dark exciton ground state promotes photon-pair emission in individual perovskite nanocrystals, *Nat. Commun.* **2020**, *11*, 6001. https://doi.org/10.1038/s41467-020-19740-7

(20) Fu, M.; Tamarat, P.; Huang, H.; Even, J.; Rogach, A. L.; Lounis, B. Neutral and Charged Exciton Fine Structure in Single Lead Halide Perovskite Nanocrystals Revealed by Magneto-optical Spectroscopy, *Nano Lett.* **2017**, *17*, 2895-2901. https://doi.org/10.1021/acs.nanolett.7b00064

(21) Yuan, G.; Ritchie, C.; Ritter, M.; Murphy, S.; Gómez, D. E.; Mulvaney, P. The Degradation and Blinking of Single CsPbI3 Perovskite Quantum Dots, *J. Phys. Chem. C* **2018**, *122*, 13407-13415. https://doi.org/10.1021/acs.jpcc.7b11168

(22) Kim, T.; Jung, S. I.; Ham, S.; Chung, H.; Kim, D. Elucidation of Photoluminescence Blinking Mechanism and Multiexciton Dynamics in Hybrid Organic–Inorganic Perovskite Quantum Dots, *Small* **2019**, *15*, 1900355, https://doi.org/10.1002/smll.201900355. https://doi.org/10.1002/smll.201900355 (accessed 2023/02/27).

(23) Seth, S.; Ahmed, T.; Samanta, A. Photoluminescence Flickering and Blinking of Single CsPbBr3 Perovskite Nanocrystals: Revealing Explicit Carrier Recombination Dynamics, *J. Phys.Chem. Lett.* **2018**, *9*, 7007-7014. https://doi.org/10.1021/acs.jpclett.8b02979

(24) Dong, Y.; Qiao, T.; Kim, D.; Parobek, D.; Rossi, D.; Son, D. H. Precise Control of Quantum Confinement in Cesium Lead Halide Perovskite Quantum Dots via Thermodynamic Equilibrium, *Nano Letters* **2018**, *18*, 3716-3722. https://doi.org/10.1021/acs.nanolett.8b00861

(25) Protesescu, L.; Yakunin, S.; Bodnarchuk, M. I.; Krieg, F.; Caputo, R.; Hendon, C. H.; Yang, R. X.; Walsh, A.; Kovalenko, M. V. Nanocrystals of Cesium Lead Halide Perovskites (CsPbX3, X = Cl, Br, and I): Novel Optoelectronic Materials Showing Bright Emission with Wide Color Gamut, *Nano Letters* **2015**, *15*, 3692-3696. https://doi.org/10.1021/nl5048779

(26) Galland, C.; Ghosh, Y.; Steinbrück, A.; Sykora, M.; Hollingsworth, J. A.; Klimov, V. I.; Htoon, H. Two types of luminescence blinking revealed by spectroelectrochemistry of single quantum dots, *Nature* **2011**, *479*, 203-207. https://doi.org/10.1038/nature10569

(27) Yuan, G.; Gómez, D. E.; Kirkwood, N.; Boldt, K.; Mulvaney, P. Two Mechanisms Determine Quantum Dot Blinking, *ACS Nano* **2018**, *12*, 3397-3405. https://doi.org/10.1021/acsnano.7b09052

(28) Makarov, N. S.; Guo, S.; Isaienko, O.; Liu, W.; Robel, I.; Klimov, V. I. Spectral and Dynamical Properties of Single Excitons, Biexcitons, and Trions in Cesium–Lead-Halide Perovskite Quantum Dots, *Nano Letters* **2016**, *16*, 2349-2362. https://doi.org/10.1021/acs.nanolett.5b05077

(29) Du, X.; Wu, G.; Cheng, J.; Dang, H.; Ma, K.; Zhang, Y.-W.; Tan, P.-F.; Chen, S. High-quality CsPbBr3 perovskite nanocrystals for quantum dot light-emitting diodes, *RSC Advances* **2017**, *7*, 10391-10396, 10.1039/C6RA27665B. http://dx.doi.org/10.1039/C6RA27665B

(30) Li, B.; Huang, H.; Zhang, G.; Yang, C.; Guo, W.; Chen, R.; Qin, C.; Gao, Y.; Biju, V. P.; Rogach, A. L.; Xiao, L.; Jia, S. Excitons and Biexciton Dynamics in Single CsPbBr3 Perovskite Quantum Dots, *J. Phys.Chem. Lett.* **2018**, *9*, 6934-6940. https://doi.org/10.1021/acs.jpclett.8b03098

(31) Becker, M. A.; Bernasconi, C.; Bodnarchuk, M. I.; Rainò, G.; Kovalenko, M. V.; Norris, D. J.; Mahrt, R. F.; Stöferle, T. Unraveling the Origin of the Long Fluorescence Decay Component of Cesium Lead Halide Perovskite Nanocrystals, *ACS Nano* **2020**, *14*, 14939-14946. https://doi.org/10.1021/acsnano.0c04401

(32) Ahmed, T.; Seth, S.; Samanta, A. Mechanistic Investigation of the Defect Activity Contributing to the Photoluminescence Blinking of CsPbBr3 Perovskite Nanocrystals, *ACS Nano* **2019**, *13*, 13537-13544. https://doi.org/10.1021/acsnano.9b07471

(33) Li, S.; Luo, J.; Liu, J.; Tang, J. Self-Trapped Excitons in All-Inorganic Halide Perovskites: Fundamentals, Status, and Potential Applications, *J. Phys.Chem. Lett.* **2019**, *10*, 1999-2007. https://doi.org/10.1021/acs.jpclett.8b03604

(34) Tao, W.; Zhang, C.; Zhou, Q.; Zhao, Y.; Zhu, H. Momentarily trapped exciton polaron in two-dimensional lead halide perovskites, *Nat. Commun.* **2021**, *12*, 1400. https://doi.org/10.1038/s41467-021-21721-3

(35) Wu, X.; Trinh, M. T.; Niesner, D.; Zhu, H.; Norman, Z.; Owen, J. S.; Yaffe, O.; Kudisch, B. J.; Zhu, X. Y. Trap States in Lead Iodide Perovskites, *Journal of the American Chemical Society* **2015**, *137*, 2089-2096. https://doi.org/10.1021/ja512833n

(36) Yang, B.; Han, K. Ultrafast Dynamics of Self-Trapped Excitons in Lead-Free Perovskite Nanocrystals, *J. Phys. Chem. Lett.* **2021**, *12*, 8256-8262. https://doi.org/10.1021/acs.jpclett.1c01828

(37) Ma, X.; Pan, F.; Li, H.; Shen, P.; Ma, C.; Zhang, L.; Niu, H.; Zhu, Y.; Xu, S.; Ye, H. Mechanism of Single-Photon Upconversion Photoluminescence in All-Inorganic Perovskite Nanocrystals: The Role of Self-Trapped Excitons, *J. Phys.Chem. Lett.* **2019**, *10*, 5989-5996. https://doi.org/10.1021/acs.jpclett.9b02289

(38) Seiler, H.; Zahn, D.; Taylor, V. C. A.; Bodnarchuk, M. I.; Windsor, Y. W.; Kovalenko, M. V.; Ernstorfer, R. Direct Observation of Ultrafast Lattice Distortions during Exciton–Polaron Formation in Lead Halide Perovskite Nanocrystals, *ACS Nano* **2023**, *17*, 1979-1988. https://doi.org/10.1021/acsnano.2c06727

(39) Cho, K.; Tahara, H.; Yamada, T.; Suzuura, H.; Tadano, T.; Sato, R.; Saruyama, M.; Hirori, H.; Teranishi, T.; Kanemitsu, Y. Exciton–Phonon and Trion–Phonon Couplings Revealed by Photoluminescence Spectroscopy of Single CsPbBr3 Perovskite Nanocrystals, *Nano Lett.* **2022**, *22*, 7674-7681. https://doi.org/10.1021/acs.nanolett.2c02970

(40) Lubin, G.; Yaniv, G.; Kazes, M.; Ulku, A. C.; Antolovic, I. M.; Burri, S.; Bruschini, C.; Charbon, E.; Yallapragada, V. J.; Oron, D. Resolving the Controversy in Biexciton Binding Energy of Cesium Lead Halide Perovskite Nanocrystals through Heralded Single-Particle Spectroscopy, *ACS Nano* **2021**, *15*, 19581-19587. https://doi.org/10.1021/acsnano.1c06624

(41) Shulenberger, K. E.; Ashner, M. N.; Ha, S. K.; Krieg, F.; Kovalenko, M. V.; Tisdale, W. A.; Bawendi, M. G. Setting an Upper Bound to the Biexciton Binding Energy in CsPbBr3 Perovskite Nanocrystals, *J. Phys. Chem. Lett.* **2019**, *10*, 5680-5686. https://doi.org/10.1021/acs.jpclett.9b02015

(42) Castañeda, J. A.; Nagamine, G.; Yassitepe, E.; Bonato, L. G.; Voznyy, O.; Hoogland, S.; Nogueira, A. F.; Sargent, E. H.; Cruz, C. H. B.; Padilha, L. A. Efficient Biexciton Interaction in Perovskite Quantum Dots Under Weak and Strong Confinement, *ACS Nano* **2016**, *10*, 8603-8609. https://doi.org/10.1021/acsnano.6b03908

(43) Yarita, N.; Tahara, H.; Ihara, T.; Kawawaki, T.; Sato, R.; Saruyama, M.; Teranishi, T.; Kanemitsu, Y. Dynamics of Charged Excitons and Biexcitons in CsPbBr3 Perovskite Nanocrystals Revealed by Femtosecond Transient-Absorption and Single-Dot Luminescence Spectroscopy, *J. Phys. Chem. Lett.* **2017**, *8*, 1413-1418. https://doi.org/10.1021/acs.jpclett.7b00326

(44) Nguyen, T. P. T.; Blundell, S. A.; Guet, C. Calculation of the biexciton shift in nanocrystals of inorganic perovskites, *Phys. Rev. B* **2020**, *101*, 125424. https://link.aps.org/doi/10.1103/PhysRevB.101.125424

(45) Aneesh, J.; Swarnkar, A.; Kumar Ravi, V.; Sharma, R.; Nag, A.; Adarsh, K. V. Ultrafast Exciton Dynamics in Colloidal CsPbBr3 Perovskite Nanocrystals: Biexciton Effect and Auger Recombination, *The Journal of Physical Chemistry C* **2017**, *121*, 4734-4739. https://doi.org/10.1021/acs.jpcc.7b00762

(46) Ashner, M. N.; Shulenberger, K. E.; Krieg, F.; Powers, E. R.; Kovalenko, M. V.; Bawendi, M. G.; Tisdale, W. A. Size-Dependent Biexciton Spectrum in CsPbBr3 Perovskite Nanocrystals, *ACS Enery Lett.* **2019**, *4*, 2639-2645. https://doi.org/10.1021/acsenergylett.9b02041

(47) Dana, J.; Binyamin, T.; Etgar, L.; Ruhman, S. Unusually Strong Biexciton Repulsion Detected in Quantum Confined CsPbBr3 Nanocrystals with Two and Three Pulse Femtosecond Spectroscopy, *ACS Nano* **2021**, *15*, 9039-9047. https://doi.org/10.1021/acsnano.1c02123

(48) Rossi, D.; Wang, H.; Dong, Y.; Qiao, T.; Qian, X.; Son, D. H. Light-Induced Activation of Forbidden Exciton Transition in Strongly Confined Perovskite Quantum Dots, *ACS Nano* **2018**, *12*, 12436-12443. https://doi.org/10.1021/acsnano.8b06649

(49) Wahl, M.; Gregor, I.; Patting, M.; Enderlein, J. Fast calculation of fluorescence correlation data with asynchronous time-correlated single-photon counting, *Optics Express* **2003**, *11*, 3583-3591. https://opg.optica.org/oe/abstract.cfm?URI=oe-11-26-3583

TOC